INVESTIGATION OF COULOMB DIFFRACTION INTERFERENCE IN ^{23}Al BREAKUP REACTION

Surender, Ravinder Kumar[†]

Department of Physics
Deenbandhu Chhotu Ram University of Science and Technology
Murthal, Sonepat, Haryana 131039, India

Received 18 February 2023, accepted 4 September 2023,
published online 15 September 2023

The presence of Coulomb diffraction interference has been investigated for single-proton breakup from ^{23}Al nucleus reaction. The study is performed for light, medium, and heavy targets *i.e.*, ^{12}C, ^{58}Ni, and ^{208}Pb cases at 40 and 80 MeV/nucleon beam energies. The Coulomb interaction between core–target and proton–target are treated to all orders, including the full-multipole expansion of the Coulomb potential, while nuclear diffraction dissociation is treated with eikonal approximation. The effects of Coulomb diffraction interference on single-proton breakup cross-section and Full Width Half Maxima (FWHM) width of core longitudinal momentum distribution (LMD) have been investigated. Interferences between the core–target (recoil interaction) and proton–target (direct interaction) Coulomb interactions are also being examined. The nature of interferences is constructive as well as destructive depending on the target atomic number and incident energy. Consequently, enhancement and reduction in breakup cross sections and the LMD widths have been observed in a significant magnitude. The interference effects for ^{58}Ni target case are found almost three to four times of that of ^{12}C and ^{208}Pb target cases. We believe that our investigation would help in planning future experiments involving proton halo breakup reactions as well as for better understanding and interpretation of experimental data of ^{23}Al breakup reaction.

DOI:10.5506/APhysPolB.54.9-A1

1. Introduction

This work is concerned with the presence of interference among the Coulomb and nuclear diffraction breakup mechanisms during single-proton breakup from ^{23}Al nucleus. The breakup reactions are caused by the Coulomb and nuclear interactions between the incoming projectile and the target nuclei, the dominating interaction mechanism causing breakup depends on

[†] Corresponding author: `drravinderkumar.phy@dcrustm.org`

the atomic number of participating target nucleus and the incident energy. Normally in breakup reactions, the interference between the Coulomb and nuclear interactions has been assumed very modest for all the targets in the medium incident energy range (40–80 MeV/nucleon), and their impact on breakup observables had generally been ignored while analyzing the experimental data. However, the fact is that during the interaction, both breakup mechanisms remain present and can interfere with one another. In this light, there have been few attempts to examine the Coulomb nuclear interference effects in breakup reactions [1–4]. Also, in theoretical studies [5, 6], the Coulomb and nuclear interactions were studied using the all-order formalism [2, 3, 7, 8], and reported the presence of dynamical effects in single-proton breakup reactions involving proton-rich exotic nuclei. Also, they have exclusively shown the interference among core–target (recoil interaction) and valence proton–target (direct interaction) Coulomb interactions. Their work for ^{8}B and ^{17}F nucleus breakup reactions demonstrated that recoil and direct interactions could over-predict or under-predict the magnitude of breakup observables (such as breakup cross section, width of core longitudinal momentum distribution, and also the proton angular distribution), these reported results were also being endorsed in later work [9].

The Coulomb dissociation mechanism is the inverse of radiative proton capture reaction, which is being used to determine the rate of reaction in proton capture reactions of astrophysical relevance. Thus, the literature consistently emphasized the need for a better understanding of the reaction mechanisms and clear analysis of experimental data for deducing several parameters related to the initial state of the projectile nucleus, spectroscopic factor *etc.* Some of these parameters are being employed as input for obtaining astrophysical information [4, 10–12]. Thus, a better understanding of the Coulomb dissociation process, especially in proton halo breakup reactions, and its interference with other breakup reaction mechanisms becomes essential for obtaining precise information about the radiative capture reactions and other astrophysical reactions.

In the present study, we theoretically investigated the presence of interference between the Coulomb and diffraction mechanisms in a single-proton removal reaction from ^{23}Al for three different targets at 40 and 80 MeV/nucleon beam energies. Specifically, we have examined the effects of Coulomb diffraction interference on single-proton breakup cross section and full-width half-maxima (FWHM) width of core longitudinal momentum distribution (LMD). All the calculations are carried out by treating the Coulomb mechanism to all orders including the full multipole expansion of the Coulomb potential and nuclear diffraction via the eikonal approximation [6, 8]. To analyze clearly the role of interference in breakup observables, we performed calculations for the Coulomb and nuclear diffraction dissociation individually (without considering the other) as well as jointly (with both mechanisms). Here, we are interested in ^{23}Al breakup reaction because it is a proton-rich nucleus lying near the proton drip line having very small proton separation energy ($S_p = 141.11(43)$ keV) [10] and large matter radii, which indicates ^{23}Al to be a halo candidate as reported in Refs. [10, 13–16]. Besides these, there are still many ambiguities related to its ground-state spin parity ($5/2^+$ or $1/2^+$), the possibility of *sd* shell mixing, level inversion, and most importantly, its astrophysical implications as pointed out in Refs. [11, 16, 17], due to which this nucleus has remained under investigation since its discovery. Secondly, in recent experimental work [10], the measured FWHM value of core fragment momentum distribution (LMD) and single-proton breakup cross section were being used as an important key input parameter for extracting the spectroscopic factor and asymptotic normalization coefficients (ANCs) [11, 18–20] which were then used to extract stellar reaction rate for direct proton capture reaction $^{22}\mathrm{Mg}(p,\gamma)^{23}\mathrm{Al}$ [10].

Therefore, keeping in view the need for precise values of breakup observables for astrophysical interest and better understanding of breakup mechanisms, as reported in Refs. [5, 6], it would be quite interesting to investigate the presence of Coulomb diffraction interference in ^{23}Al nucleus breakup reaction and its influence on single-proton breakup cross section and the FWHM width of core longitudinal momentum distribution.

2. Theoretical formalism

Following the theoretical formalism developed in Refs. [6, 8], we have investigated the single-proton breakup from ^{23}Al nucleus on different targets at different incident energies. Wherein the Coulomb potential between projectile and target is taken as

$$V\left(\vec{r},\vec{R}\right) = \frac{V_{\mathrm{c}}}{\left|\vec{R}-\beta_1\vec{r}\right|} + \frac{V_{\mathrm{v}}}{\left|\vec{R}+\beta_2\vec{r}\right|} - \frac{V_0}{\vec{R}}\,, \tag{1}$$

where $V_{\mathrm{c}} = Z_{\mathrm{c}}Z_{\mathrm{t}}e^2$, $V_{\mathrm{v}} = Z_{\mathrm{v}}Z_{\mathrm{t}}e^2$, and $V_0 = (Z_{\mathrm{v}}+Z_{\mathrm{c}})\,Z_{\mathrm{t}}e^2$. β_1 and β_2 are the mass ratios of the proton and core, respectively, to that of the projectile and Z_{c}, Z_{t}, and Z_{v} are the core, target, and valence proton charges respectively. The geometry of the system is shown in Fig. 1. Following the procedure of Ref. [2], the Coulomb phase in perturbation formalism for the whole projectile is

$$\begin{aligned}\chi^{\mathrm{p}} \;=\; & \frac{2}{\hbar v}\Big(V_{\mathrm{c}}\,\mathrm{e}^{i\beta_1\omega z/v}K_0\left(\omega b_{\mathrm{c}}/v\right) - V_0K_0\left(\omega R_{\perp}/v\right) \\ & +V_{\mathrm{v}}\,\mathrm{e}^{-i\beta_2\omega z/v}K_0\left(\omega b_{\mathrm{v}}/v\right)\Big)\,,\end{aligned} \tag{2}$$

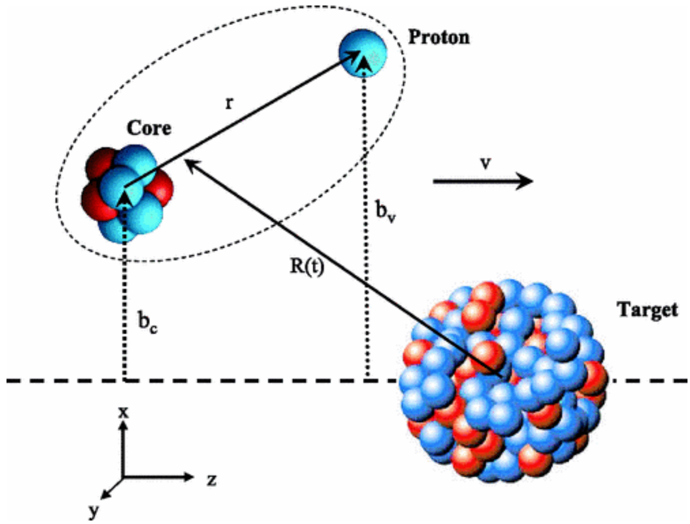

Fig. 1. Geometry of the interaction.

where $\omega = (\varepsilon_f - \varepsilon_0)/\hbar$, ε_0 and ε_f are the valence nucleon binding energy and final nucleon–core continuum energy, and K_0 is the usual modified Bessel function. Thus, the whole projectile Coulomb potential (V_0) can be simply written as a sum of core target potential (V_c) and valence proton target potential (V_v) *i.e.*, $V_0 = V_c + V_v$, therefore, the whole projectile Coulomb phase in perturbation formalism can be written as

$$\chi^{\mathrm{p}} = \chi(\beta_1, V_{\mathrm{c}}) + \chi(-\beta_2, V_{\mathrm{v}}) \,, \tag{3}$$

where

$$\chi(\beta_1, V_{\mathrm{c}}) = \frac{2V_{\mathrm{c}}}{\hbar v}\left(\mathrm{e}^{i\beta_1\omega z/v} K_0\left(\frac{\omega b_{\mathrm{c}}}{v}\right) - K_0\left(\frac{\omega R_\perp}{v}\right)\right) , \tag{4}$$

$$\chi(-\beta_2, V_{\mathrm{v}}) = \frac{2V_{\mathrm{v}}}{\hbar v}\left(\mathrm{e}^{-i\beta_2\omega z/v} K_0\left(\frac{\omega b_{\mathrm{v}}}{v}\right) - K_0\left(\frac{\omega R_\perp}{v}\right)\right) . \tag{5}$$

In the whole projectile Coulomb phase (Eq. (3)), the first term describes the core target Coulomb interaction called recoil of the core, whereas the second term describes the proton–target Coulomb interaction known as the direct interaction. García-Camacho *et al.* [8] and Margueron *et al.* [7], and references therein, have stressed the importance of inclusion of the Coulomb potential to all orders in proton halo breakup reactions and also suggested that higher-order terms are easier and more accurate to calculate in sudden approximation. In their proposed technique, all orders in sudden approximation are achieved by replacing the first-order sudden term, which diverges for large impact parameter by the first-order time-dependent perturbation term, details of the technique are discussed in Refs. [2, 3, 7, 8]. Therefore, following this technique, we have also treated the Coulomb potential to all orders in sudden formalism exclusively for both core–target (recoil) and proton–target (direct) interactions where respective amplitudes are

$$g^{\mathrm{rec}}(b_{\mathrm{c}}) = \int \mathrm{d}\vec{r}\,\mathrm{e}^{-i\vec{k}\cdot\vec{r}}\phi_i(\vec{r})\left(\mathrm{e}^{i\frac{2V_{\mathrm{c}}}{\hbar v}\log\frac{b_{\mathrm{c}}}{R_\perp}} - 1 - i\frac{2V_{\mathrm{c}}}{\hbar v}\log\frac{b_{\mathrm{c}}}{R_\perp} + i\chi(\beta_1, V_{\mathrm{c}})\right), \tag{6}$$

$$g^{\mathrm{dir}}(b_{\mathrm{v}}) = \int \mathrm{d}\vec{r}\,\mathrm{e}^{-i\vec{k}\cdot\vec{r}}\phi_i(\vec{r})\left(\mathrm{e}^{i\frac{2V_{\mathrm{v}}}{\hbar v}\log\frac{b_{\mathrm{v}}}{R_\perp}} - 1 - i\frac{2V_{\mathrm{v}}}{\hbar v}\log\frac{b_{\mathrm{v}}}{R_\perp} + i\chi(-\beta_2, V_{\mathrm{v}})\right), \tag{7}$$

where $\chi(\beta_1, V_{\mathrm{c}})$ and $\chi(-\beta_2, V_{\mathrm{v}})$ are the first-order time-dependent perturbed Coulomb phases for the core–target and proton–target interactions, calculated using Eqs. (4) and (5). The nuclear diffraction dissociation amplitude in eikonal approximation is calculated by

$$g^{\mathrm{diff}} = \int \mathrm{d}\vec{r}\,\mathrm{e}^{-i\vec{k}\cdot\vec{r}}\phi_i(\vec{r})|S_{\mathrm{pt}}(b_{\mathrm{v}}) - 1|\,. \tag{8}$$

These Coulomb and nuclear diffraction amplitudes are used to calculate the core fragment momentum distribution as follows:

$$\frac{\mathrm{d}\sigma}{\mathrm{d}\vec{k}} = \frac{1}{8\pi^3}\int \mathrm{d}\vec{b}_{\mathrm{c}}\,|S_{\mathrm{ct}}(b_{\mathrm{c}})|^2\left|g^{\mathrm{rec}} + g^{\mathrm{dir}} + g^{\mathrm{diff}}\right|^2, \tag{9}$$

where $\phi_i(\vec{r})$, $S_{\mathrm{ct}}(b_c)$, and $S_{\mathrm{pt}}(b_v)$ are the projectile wave function, core–target, and proton–target interaction S-matrices respectively. The S-matrices are calculated using the MOMDIS code [21] in $t\rho\rho$ formalism using the Hartree–Fock [22] and $2pF$ nuclear density forms of the core and target nucleus respectively [23]. The single-proton breakup cross sections are calculated by integrating the longitudinal momentum distribution over the momentum, whereas the projectile's bound state wave function, $\phi_i(\vec{r})$, is calculated by numerically solving the Schrödinger wave equation using the Woods–Saxon nuclear potential of fixed geometry *i.e.*, radius ($r_0 = 1.25$ fm), diffuseness ($a_0 = 0.7$ fm) [10], and $V_{ls} = -20.72$ MeV [24, 25] for the considered bound state projectile configurations. The depths of nuclear potentials are adjusted to reproduce the effective binding energies of the valence proton *i.e.*, $S_p^{\mathrm{eff}} = E_{\mathrm{c}}^{\mathrm{ex}} + S_p$, ($E_{\mathrm{c}}^{\mathrm{ex}}$, and S_p being the excitation energy of core and valence proton separation energy *i.e.* ($S_p = 0.141$ MeV) respectively).

We keep in view that the single-proton breakup cross section and core longitudinal momentum distribution (LMD) width are sensitive to the values of the Woods–Saxon potential parameter (radius (r_0) and diffuseness (a_0)) used in the projectile wave function. Thus, before proceeding to the final calculations, we have cross-checked the sensitivity of breakup cross section and LMD width on these Woods–Saxon nuclear potential parameters for $[0^+ \otimes 1d_{5/2}]$ projectile configuration case at 40 MeV/nucleon beam energy. We found that cross section increases by approximately 20% as the value of r_0 varied from 1.15 to 1.3 fm, while the FWHM width of LMD increases by 2–3%. On the other hand, an increase in cross section is observed at less than 10% with variation in the a_0 value from 0.6 to 0.7 fm and increase in the LMD width is less than 2–3%. We have also checked that the cross section and FWHM width of LMD varies less than 5% and 2%, respectively, if we double the proton separation energy *i.e.* 0.282 MeV. These observed sensitivities are consistent with the results of Ref. [26]. The full theoretical details of formalism are discussed in Refs. [2, 3, 7, 8].

3. Calculations and results

Using the theoretical formalism discussed in Section 2, we have exclusively investigated the presence of interference between Coulomb (total) (direct plus recoil interaction) and nuclear diffraction mechanisms, and also the interference between direct and recoil Coulomb interactions in a single-proton breakup from ^{23}Al nucleus reaction. Quantitatively, we have examined the effect of interference on the breakup cross section and FWHM of LMD width. The Coulomb interaction between valence proton–target (direct) and core–target (recoil) is calculated using the all-orders formalism, including the full multipole expansion of the Coulomb potential while nuclear diffraction dissociation by eikonal approximation, as briefly discussed above and in detail in Refs. [2, 3, 7, 8]. Here, the investigation is performed for light, medium, and heavy target cases, *i.e.* ^{12}C, ^{58}Ni, and ^{208}Pb at two commonly used incident energies *i.e.*, 40 and 80 MeV/nucleon. We calculated separately and jointly the single-proton breakup cross section and core fragment longitudinal momentum distribution (LMD) due to nuclear diffraction and the Coulomb breakup (including recoil and direct interactions) for both considered projectile configurations. Here, we have not included the proton stripping contribution in the interference study because in the stripping mechanism, valence nucleon is stripped off by the target in the sense of optical model absorption and its energy degraded such that it would not be detected in coincidence with the core, so such mechanisms neither interfere with diffraction nor with the Coulomb breakup mechanism.

For simplicity, we assumed that ^{23}Al nucleus has a core plus valence proton nuclear structure, *i.e.* (^{22}Mg+p) having either core in the ground state (0^+) ($E_c^{ex} = 0$ MeV) or the first excited state (2^+) ($E_c^{ex} = 1.247$ MeV) coupled with $d_{5/2}$ state of valence proton, so as per shell model prediction, there are $[0^+ \otimes 1d_{5/2}]$ and $[2^+ \otimes 1d_{5/2}]$ projectile bound state configurations, producing the ground state of ^{23}Al ($J^\pi = (5/2)^+$) [10]. We have not considered the other experimentally observed core excited states *i.e.*, 4_1^+ ($E_c^{ex} = 3.308$ MeV) and 4_2^+ ($E_c^{ex} = 5.293$ MeV) in our calculations due to their very small contribution as reported in Ref. [10]. Here, we have used spectroscopic factor as unity for both the considered projectile configurations throughout the calculations. The percentage variation in observable values caused by interference of breakup mechanisms is shown in tables and calculated using the formula *i.e.* % Interference $= ((X^{\text{Coul+Diff}} - (X^{\text{Coul}} + X^{\text{Diff}}))/(X^{\text{Coul+Diff}})) \times 100\%$, where X stands for the breakup cross section or FWHM width of LMD.

The calculated FWHM width of core longitudinal momentum distribution and single-proton breakup cross section values are depicted in Tables 1–4. The results of $[0^+ \otimes 1d_{5/2}]$ projectile configuration for ^{12}C, ^{58}Ni, and ^{208}Pb targets at 40 and 80 MeV/nucleon incident energies are shown in Table 1, and the respective longitudinal momentum distribution spectrums are shown in

Table 1. Calculated the single-proton breakup cross section and LMD width for diffraction, Coulomb (total) (contain direct and recoil term), the simple sum of Coulomb (total) and diffraction mechanism, and Coulomb (total) plus diffraction (calculated together) for $[0^+ \otimes 1d_{5/2}]$ projectile state with different targets at 40 and 80 MeV/nucleon beam energy.

Target	^{12}C		^{58}Ni		^{208}Pb	
E_{inc} [MeV/nucleon]	40	80	40	80	40	80
Diff. [mb]	10.37	13.65	14.95	20.04	21.45	29.26
Coul. (total) [mb]	5.27	3.99	113.07	66.92	2009.91	821.52
Coul.+Diff. (simple sum) [mb]	15.64	17.64	128.02	86.96	2031.36	850.29
Coul.+Diff. (Cal. together) [mb]	16.42	16.20	156.90	105.04	2077.98	927.91
% Interference	+4.99	−8.16	+22.50	+20.79	+2.29	+9.13
	FWHM [MeV/c]					
Diff.	164.24	177.59	156.54	167.08	153.73	163.91
Coul. (total)	121.33	140.53	113.73	120.44	145.80	129.77
Coul.+Diff. (simple sum)	145.49	165.91	117.46	127.72	145.92	130.79
Coul.+Diff. (Cal. together)	144.54	162.20	125.44	132.23	152.13	138.19
% Interference	−0.65	−2.24	+6.79	+3.53	+4.25	+5.66

Fig. 2. Calculated longitudinal momentum distribution for diffraction (blue dashed curve), Coulomb (total) (red dotted curve containing both direct and recoil terms) and Coulomb (total) calculated with diffraction mechanism (black solid curve containing all interferences between diffraction, direct, and recoil Coulomb terms), and the simple algebraic sum of Coulomb (total) and diffraction (green dash-dotted curve), calculated separately in the absence of each other and then simply added together, are shown in Fig. 2 (a)–(f) and respective breakup cross section values are revealed in Table 1. It is clear that for ^{12}C target case, at 40 MeV/nucleon, the simple sum of Coulomb and diffraction (green dash-dotted curve) is smaller than the Coulomb plus diffraction calculated together (black solid curve) (Fig. 2 (a)), which indicates the presence of constructive interference between the Coulomb and diffraction mechanisms. However, at 80 MeV/nucleon, the order of the cross section is inverted (Fig. 2 (d)), indicating destructive in-

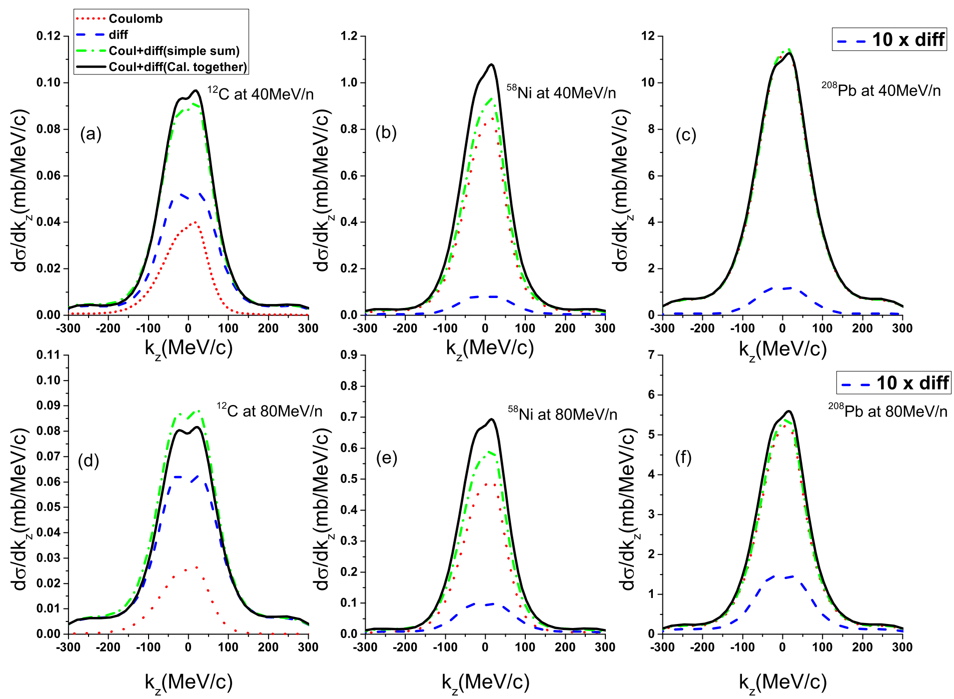

Fig. 2. LMD distribution of core fragment for the $[0^+ \otimes 1d_{5/2}]$ projectile configuration for: diffraction (blue dashed curve, magnified 10 times for the sake of visibility in panels (c) and (f)), Coulomb (total) (including direct and recoil term) mechanism (red dotted curve), Coulomb plus diffraction (calculated together) (black solid curve), and the simple sum of Coulomb and diffraction mechanism (green dash-dotted curve) at 40 and 80 MeV/nucleon beam energies for ^{12}C, ^{58}Ni, and ^{208}Pb target.

terference. As a consequence, the respective values of single-proton breakup cross section (shown in Table 1) show an enhancement and reduction in the absolute values of breakup cross section by +4.99% and −8.16% respectively, while the FWHM width of LMD reduces by −0.65% to −2.24% for 40 and 80 MeV/nucleon incident energies. The variation in cross section and LMD width are found mildly sensitive to the incident energy. However, in the case of ^{58}Ni and ^{208}Pb targets (Fig. 2 (b), (e) and Fig. 2 (c), (f)), the Coulomb plus diffraction cross section calculated together (black solid curve) is mostly seen bigger than the Coulomb and diffraction simple sum cross section (green dash-dotted curve), which indicates the presence of constructive interference between the Coulomb and diffraction for both the incident energies. For ^{58}Ni, the enhancement in the breakup cross-section values is found almost +(22 or 20)% for both the incident energies and is almost insensitive to the incident energy. On the other hand, for ^{208}Pb target, the enhancement in cross section is found +2.29% to +9.13%, and it increases with the incident energy. Regarding the variation in the FWHM width of LMD, an enhancement of +6.79% to +3.53% and +4.25% to +5.66% at 40 and 80 MeV/nucleon incident energies are observed for ^{58}Ni and ^{208}Pb targets, respectively. Here, the variation in FWHM of LMD width due to interference is found slightly sensitive to the incident energy.

A similar trend of results is observed for the $[2^+ \otimes 1d_{5/2}]$ projectile configuration. The LMD spectrum for different target cases at 40 and 80 MeV/nucleon incident energies is shown in Fig. 3, and the respective breakup cross section and FWHM widths are shown on the top and bottom side of Table 2. For ^{12}C target at 40 MeV/nucleon energy (Fig. 3 (a)), the Coulomb and diffraction calculated together (black solid curve) is found bigger than the simple sum of Coulomb and diffraction (green dash-dotted curve), while at 80 MeV/nucleon (Fig. 3 (d)), the Coulomb and diffraction calculated together (black solid curve) is smaller than the simple sum of Coulomb and diffraction (green dash-dotted curve), which shows the constructive and destructive interference which enhance and reduce the breakup cross section by +5% and −8.16% at 40 and 80 MeV/nucleon, respectively. At the same time, due to the Coulomb diffraction interference, the FWHM of LMD reduced by −0.62% to −1.52% at 40 and 80 MeV/nucleon, respectively. For ^{58}Ni and ^{208}Pb target cases, again the Coulomb and diffraction calculated together (black solid curve) is found bigger than the simple sum of Coulomb and diffraction (green dash dotted curve) showing the constructive interference between the Coulomb and diffraction mechanism, which increases the breakup cross section by +26.72% and +23.12% for ^{58}Ni and +4.12% and +11.75% for ^{208}Pb target at 40 and 80 MeV/nucleon incident energy respectively. On the other hand, the FWHM width of LMD increases by +4.69% and +2.59% for ^{58}Ni and +0.82% and +2.04% for ^{208}Pb target at 40 and 80 MeV/nucleon respectively. The variation in FWHM of LMD with the incident energy is observed mild for all the target cases. It is also observed for both the projectile configurations that for the light target (^{12}C), the Coulomb diffraction interference is constructive at 40 MeV/nucleon energy which increases the absolute value of cross section, while at high energy, it shows destructive behavior which reduce the cross section, but in medium- and heavy-mass target *i.e.* ^{58}Ni, or ^{208}Pb cases, the interference is always found of constructive nature. However, its percentage varies with the incident energy (as can be seen in Tables 1 and 2). It is important to mention that in the case of medium target, the percentage of Coulomb diffraction constructive interference is highest at approximately 22% to 26%, while for other (light and heavy targets), this percentage is hardly laying below or near 10% for both the considered projectile configurations. This behavior looks reasonable because in the medium-mass target case, both the nuclear diffraction and Coulomb mechanism contribute equally to the breakup, so

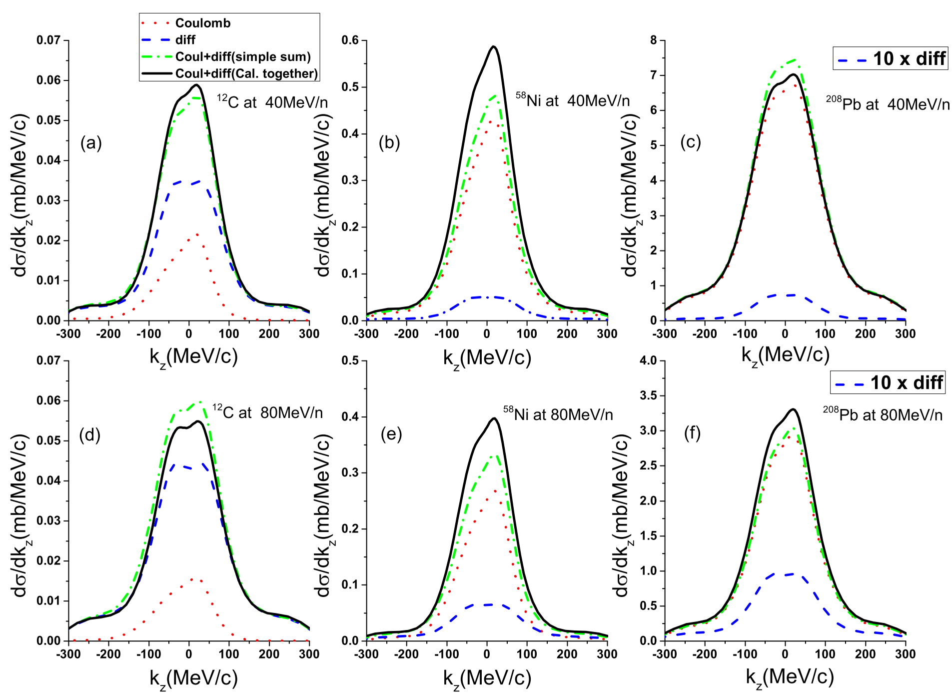

Fig. 3. LMD distribution of core fragment for the $[2^+ \otimes 1d_{5/2}]$ projectile configuration for: diffraction (blue dashed curve), Coulomb (total) (recoil and direct calculated together) mechanism (red dotted curve), Coulomb plus diffraction (calculated together) (black solid curve), and simple sum of Coulomb and diffraction mechanism (green dash-dotted curve) spectrums at 40 and 80 MeV/nucleon beam energies with ^{12}C, ^{58}Ni, and ^{208}Pb target.

the possibility of interference between the Coulomb and diffraction mechanisms is higher in comparison to light target, where only the nuclear interaction dominates over the Coulomb mechanism or in the heavy target, where the Coulomb mechanism dominates over the nuclear mechanism.

Table 2. Calculated the single-proton breakup cross section and LMD width corresponding to diffraction, Coulomb (total) (recoil and direct calculated together), the simple sum of Coulomb (total) and diffraction mechanisms, and Coulomb (total) plus diffraction (calculated together) for the projectile state $[2^+ \otimes 1d_{5/2}]$ with different targets at 40 and 80 MeV/nucleon beam energy.

Target	^{12}C		^{58}Ni		^{208}Pb	
E_{inc} [MeV/nucleon]	40	80	40	80	40	80
Diff. [mb]	7.85	11.02	10.82	15.46	15.28	22.34
Coul. (total) [mb]	2.95	2.46	68.07	40.03	1526.44	573.62
Coul.+Diff. (simple sum) [mb]	10.80	13.48	78.89	55.49	1541.72	595.96
Coul.+Diff. (Cal. together) [mb]	11.34	12.38	99.97	68.32	1605.37	666.01
% Interference	+5.00	−8.16	+26.72	+23.12	+4.12	+11.75
	FWHM [MeV/c]					
Diff.	185.99	202.15	177.85	192.07	175.18	189.19
Coul. (total)	129.31	147.65	135.02	135.86	190.93	164.50
Coul.+Diff. (simple sum)	164.33	187.11	140.07	146.40	190.72	165.40
Coul.+Diff. (Cal. together)	163.31	184.27	146.64	150.20	192.29	168.78
% Interference	−0.62	−1.52	+4.69	+2.59	+0.82	+2.04

Thus, this observation indicates important information that while planning future experiments (to avoid interference effects), the target should be chosen either light (small atomic number) or heavy (large atomic number). Our calculated results look consistent with the results of Ref. [3], wherein the angular distribution of neutrons was studied and the highest constructive interference was reported for the medium-mass target (^{48}Ti) in comparison to that of the light or heavy target *i.e.*, ^{197}Au and ^{208}Pb for ^{11}Be breakup reaction, while destructive interference was reported for the heavy-target cases. In our calculations for the heavy target, we observed constructive behavior of interference which is due to the fact that interaction situations are more complicated in the proton halo than in the neutron halo case. Therefore, it is also interesting to analyze exclusively the role of Coulomb interaction of valence proton with the target (direct interaction) and of the core with the target (recoil interaction) during the proton halo breakup reactions, as well as their interference effect on the Coulomb breakup cross section and width of the LMD spectrum. The calculated value of the breakup cross section corresponding to direct, recoil, their simple algebraic sum, and calculated together are shown in Tables 3 and 4, and the respective LMD spectrums are shown in Figs. 4 and 5. In the LMD spectrums of $[0^+ \otimes 1d_{5/2}]$ and $[2^+ \otimes 1d_{5/2}]$ projectile's configurations LMD Spectrums, the recoil interaction is marked with the blue dotted curve, direct interaction with the green dashed curve, the simple algebraic sum of direct and recoil curves with the red dash-dotted curve, and the Coulomb (total) (containing both direct and recoil interaction together) with the black solid curve. It is clear from Figs. 4 and 5 that the black solid curve (when direct and recoil are calculated together) is always smaller than that of the red dash-dotted curve (the simple algebraic sum of direct and recoil) which indicates the presence of destruc-

Table 3. Calculated breakup cross section for recoil, direct, the simple sum of recoil and direct, and Coulomb (total) (recoil and direct calculated together) mechanisms for the $[0^+ \otimes 1d_{5/2}]$ projectile configuration on different targets at 40 and 80 MeV/nucleon beam energies.

Target	^{12}C		^{58}Ni		^{208}Pb	
E_{inc} [MeV/nucleon]	40	80	40	80	40	80
Recoil [mb]	4.11	3.30	66.30	52.99	453.71	345.03
Direct [mb]	17.13	12.75	251.53	195.67	1995.78	1300.12
Recoil+Direct (simple sum) [mb]	21.23	16.07	317.82	248.67	2449.50	1645.16
Coulomb (Recoil+Direct) [mb] (Cal. together) [mb]	5.27	3.99	113.07	66.92	2009.91	821.52
% Interference	−75.18	−75.17	−64.42	−73.09	−17.95	−50.06

Table 4. Calculated breakup cross section for recoil, direct, the simple sum of recoil and direct, and Coulomb (total) (recoil and direct calculated together) mechanisms for the $[2^+ \otimes 1d_{5/2}]$ initial state on different targets at 40 and 80 MeV/nucleon beam energies.

Target	^{12}C		^{58}Ni		^{208}Pb	
E_{inc} [MeV/nucleon]	40	80	40	80	40	80
Recoil [mb]	2.11	1.98	30.27	28.60	206.51	170.98
Direct [mb]	8.44	7.70	123.51	108.18	1200.04	720.21
Recoil+Direct (simple sum) [mb]	10.55	9.68	153.78	136.79	1406.54	891.20
Coulomb (Recoil+Direct) [mb] (Cal. together) [mb]	2.95	2.46	68.07	40.03	1526.44	573.62
% Interference	−72.04	−74.59	−55.73	−70.74	+8.52	−35.63

tive interference between direct and recoil terms, which ultimately reduces the size and shape of the LMD curve and decreases the overall Coulomb breakup cross section as shown in Tables 3 and 4. Also, it is to be noted that the direct interaction curve (green dashed), which is proportional to β_2 (mass ratio of core to projectile), is always larger in absolute value than the recoil curve (blue dotted), giving more cross section as can be seen in Tables 3 and 4. The decrease in Coulomb (total) breakup cross section is brought on by the result of destructive interference between direct and recoil interaction terms. Also, the small asymmetries (at the top of the spectrum) in Figs. 4 and 5 are caused by direct and recoil interference. The percentage variation in destructive interference is found sensitive to the target size and its magnitude grows with projectile incident energy, especially when the target is medium or heavy in size (high atomic number). This pattern of direct and recoil interference is found consistent with the finding of Refs. [5, 6].

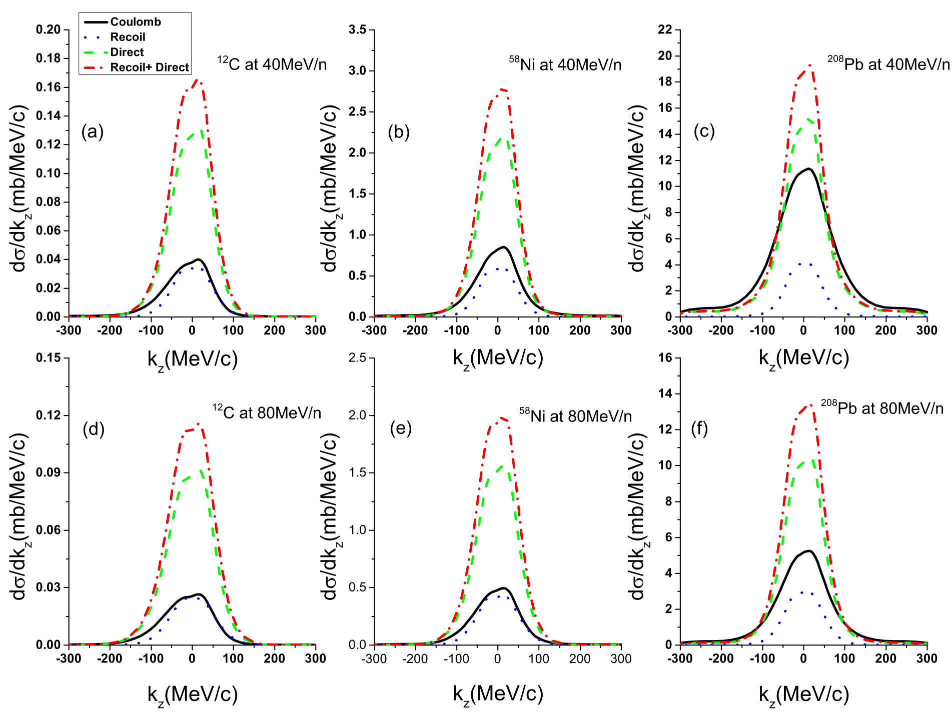

Fig. 4. LMD distribution of core fragment for the $[0^+ \otimes 1d_{5/2}]$ configuration for: Coulomb (total) (black solid curve) (recoil and direct calculated together), direct (green dashed curve), recoil (blue dotted curve), and the simple sum of recoil and direct terms (calculated separately) (red dash-dotted curve) at 40 and 80 MeV/nucleon incident energy with ^{12}C, ^{58}Ni, and ^{208}Pb target.

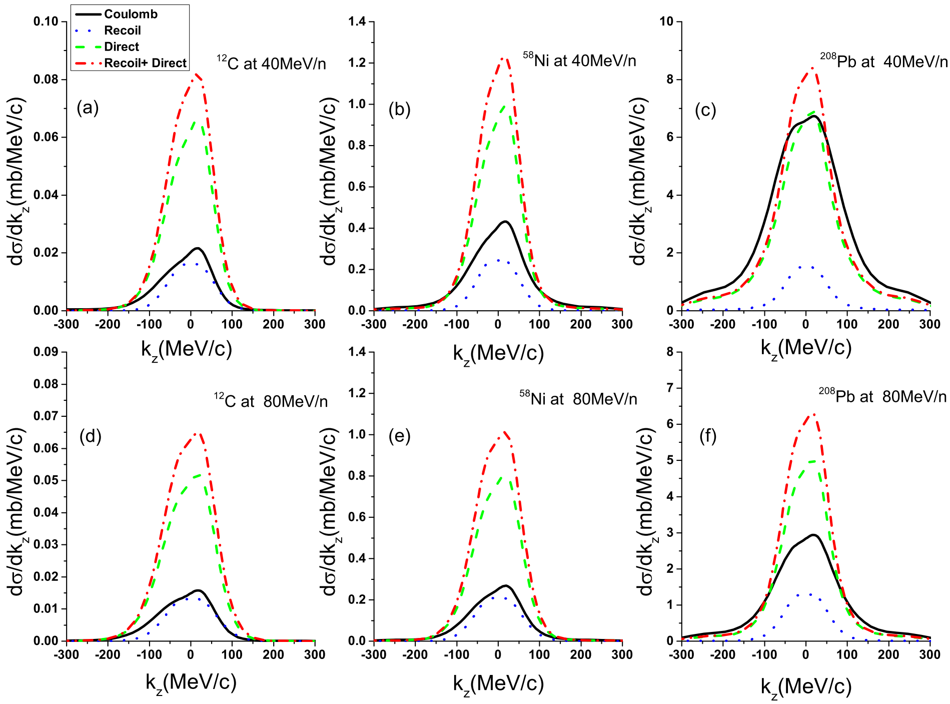

Fig. 5. LMD distribution of core fragment for the $[2^+ \otimes 1d_{5/2}]$ configuration for: Coulomb (total) (black solid curve) (recoil and direct calculated together), direct (green dashed curve), recoil (blue dotted curve), and the simple sum of recoil and direct terms (calculated separately) (red dash-dotted curve) at and 80 MeV/nucleon incident energy with ^{12}C, ^{58}Ni, and ^{208}Pb target.

4. Conclusions

Using a semi-classical method of treating both nuclear diffraction and Coulomb breakup to all orders including all multi-polarities [2, 5, 6, 8], we have for the first time quantitatively studied the presence of Coulomb diffraction interference in ^{23}Al breakup reaction. More specifically, we have investigated the effect of interference on single-proton breakup cross section and the FWHM width of longitudinal momentum distribution of the residual core fragment. We performed calculations for the light, medium, and heavy targets, *i.e.*,^{12}C, ^{58}Ni, and ^{208}Pb target at 40 and 80 MeV/nucleon incident energies because frequently more experiments are performed with these targets at these incident energies. In both light- and heavy-target cases, it is found that the Coulomb diffraction interference can influence the magnitude of a single-proton breakup cross section around 10% either through constructive or destructive behavior, while this effect is around 22%, for the medium-size target. However, the effect of interference on the LMD width is found less than 2% for ^{12}C and around 6% for ^{58}Ni and ^{208}Pb targets, this observation again endorse the fact that the LMD width is more reliable observable for halo structural investigations. It is also observed for each target that the magnitude of interference is sensitive to the incident energy of the projectile.

On the other hand, analysis of the direct and recoil Coulomb interference reveals that interference is primarily destructive for both the considered projectile configurations for all the target cases, which affects the shape, size, width of the LMD spectrum and, subsequently, reduces the total Coulomb breakup cross section as reported in Refs. [5, 6] for ^{8}B and ^{17}F nucleus breakup reactions. Additionally, it has also been noticed that both the projectile configurations exhibit almost similar patterns of the Coulomb diffraction interference in the breakup cross section and LMD width. Further, we feel that the examination of this effect for low angular momentum configurations would be more intriguing and will be discussed in forthcoming work.

Finally, we conclude that both Coulomb-diffraction and direct-recoil interferences have a non-ignorable impact on the magnitude of the breakup observables and depend very much on the target and incident energy. These interferences can introduce enhancement or reduction in the magnitude of the breakup cross section and FWHM width of longitudinal momentum distribution. We hope that this work will be helpful for a better understanding of the interplay between Coulomb and nuclear breakup mechanisms, and also for interpretation of experimental data of ^{23}Al nucleus breakup reaction.

REFERENCES

[1] A. Akhieser, A. Sitenko, «Diffractional scattering of fast deuterons by nuclei», *Phys. Rev.* **106**, 1236 (1957).

[2] A. García-Camacho, A. Bonaccorso, D.M. Brink, «All orders breakup of heavy exotic nuclei in a semiclassical model», *Nucl. Phys. A* **776**, 118 (2006).

[3] J. Margueron, A. Bonaccorso, D.M. Brink, «Coulomb-nuclear coupling and interference effects in the breakup of halo nuclei», *Nucl. Phys. A* **703**, 105 (2002).

[4] G. Baur, H. Rebel, «Coulomb breakup of nuclei — applications to astrophysics», *Annu. Rev. Nucl. Part. Sci.* **46**, 321 (1996).

[5] R. Kumar, A. Bonaccorso, «Dynamical effects in proton breakup from exotic nuclei», *Phys. Rev. C* **84**, 014613 (2011).

[6] R. Kumar, A. Bonaccorso, «Interplay of nuclear and Coulomb effects in proton breakup from exotic nuclei», *Phys. Rev. C* **86**, 061601 (2012).

[7] J. Margueron, A. Bonaccorso, D.M. Brink, «A non-perturbative approach to halo breakup», *Nucl. Phys. A* **720**, 337 (2003).

[8] A. García-Camacho, G. Blanchon, A. Bonaccorso, D.M. Brink, «All orders proton breakup from exotic nuclei», *Phys. Rev. C* **76**, 014607 (2007).

[9] Y. Kucuk, A.M. Moro, «Exclusive breakup of ^{17}F on ^{58}Ni and ^{208}Pb within the continuum-discretized coupled-channels method», *Phys. Rev. C* **86**, 034601 (2012).

[10] A. Banu *et al.*, «Structure of ^{23}Al from the one-proton breakup reaction and astrophysical implications», *Phys. Rev. C* **84**, 015803 (2011).

[11] X.-Y. Li, B. Guo, Z.-H. Li, W.-P. Liu, «Astrophysical ^{22}Mg$(p,\gamma)^{23}$Al reaction rates from asymptotic normalization coefficient of $^{23}\mathrm{Ne} \to {}^{22}\mathrm{Ne} + n$», *Chinese Phys. C* **44**, 074001 (2020).

[12] A. Horváth *et al.*, «Cross Section for the Astrophysical ^{14}C$(n,\gamma)^{15}$C Reaction via the Inverse Reaction», *Astrophys. J.* **570**, 926 (2002).

[13] C. Xiang-Zhou *et al.*, «Total Reaction Cross Section Measurements at Intermediate Energy for the Proton Halo Candidate ^{23}Al and Its Neighbours», *Chinese Phys. Lett.* **18**, 1189 (2001).

[14] A. Ozawa *et al.*, «Measurement of the spin and magnetic moment of ^{23}Al», *Phys. Rev. C* **74**, 021301 (2006).

[15] X. Cai *et al.*, «Existence of a proton halo in ^{23}Al and its significance», *Phys. Rev. C* **65**, 024610 (2002).

[16] R. Panda, M. Panigrahi, M.K. Sharma, S. Patra, «Evidence of a proton halo in ^{23}Al: A mean field analysis», *Phys. Atom. Nucl.* **81**, 417 (2018).

[17] T. Gomi *et al.*, «Coulomb dissociation experiment for explosive hydrogen burning: study of the ^{22}Mg$(p,\gamma)^{23}$Al reaction», *J. Phys. G: Nucl. Part. Phys.* **31**, S1517 (2005).

[18] F. De-Qing *et al.*, «One-Proton Halo Structure in ^{23}Al», *Chinese Phys. Lett.* **22**, 572 (2005).

[19] D. Fang *et al.*, «Examining the exotic structure of the proton-rich nucleus ^{23}Al», *Phys. Rev. C* **76**, 031601 (2007).

[20] Y.-L. Zhao, Z.-Y. Ma, B.-Q. Chen, W.-Q. Shen, «Halo Structure of Nucleus ^{23}Al», *Chinese Phys. Lett.* **20**, 53 (2003).

[21] C. Bertulani, A. Gade, «MOMDIS: a Glauber model computer code for knockout reactions», *Comput. Phys. Commun.* **175**, 372 (2006).

[22] Brookhaven National Laboratory, National Nuclear Data Center, «NuDat (Nuclear Structure and Decay Data)», March 18, 2008.

[23] L.C. Chamon *et al.*, «Toward a global description of the nucleus–nucleus interaction», *Phys. Rev. C* **66**, 014610 (2002).

[24] W. Horiuchi, Y. Suzuki, P. Capel, D. Baye, «Probing the weakly-bound neutron orbit of ^{31}Ne with total reaction and one-neutron removal cross sections», *Phys. Rev. C* **81**, 024606 (2010).

[25] A. Bohr, B.R. Mottelson, «Nuclear Structure», Vol. 1, *W.A. Benjamin*, New York 1969.

[26] Y. Zhao *et al.*, «One-proton knockout from ^{16}C at around 240 MeV/nucleon», *Phys. Rev. C* **100**, 044609 (2019).